2018

Detailed Thermal Model of an Open-Drive Single-Screw Expander for ORC Applications

Davide Ziviani
School of Mechanical Engineering, Ray W. Herrick Laboratories, Purdue University, dziviani@purdue.edu

Michel De Paepe
michel.depaepe@ugent.be

James E. Braun
Purdue University - Main Campus, jbraun@purdue.edu

Eckhard A. Groll
Purdue University - Main Campus, groll@purdue.edu

Follow this and additional works at: https://docs.lib.purdue.edu/icec

Detailed Thermal Model of Open-Drive Single-Screw Expanders for ORC Applications

Davide ZIVIANI[1*], Michel DE PAEPE[2], James E. BRAUN[1], Eckhard A. GROLL[1]

[1] Ray W. Herrick Laboratories, School of Mechanical Engineering, Purdue University
West Lafayette, 47907-2099, USA
[2] Ghent University, Department of Flow, Heat and Combustion Mechanics,
Ghent, 9000, Belgium
dziviani@purdue.edu, michel.depaepe@ugent.be, jbraun@purdue.edu, groll@purdue.edu

* Corresponding Author

ABSTRACT

A comprehensive mechanistic model of an open-drive single-screw expander for waste heat recovery applications by means of an Organic Rankine Cycle (ORC) has been previously developed and validated by the authors. The model included sub-models of geometry, leakage flows, in-chamber heat transfer, simplified friction losses and a single-lumped temperature overall energy balance. Furthermore, a non-symmetric approach was also implemented to simulate the simultaneous expansion process occurring on both side of the central rotor. In this work, the mechanistic model has been extended to compute the loads on the starwheels bearings as well as the main rotor. Forces and moments analyses allowed integration of a more detailed friction loss analysis and identification of a thermal resistance network of the housing with multiple lumped temperatures. To the best of the author's knowledge such a detailed integrated thermal model of a single-screw machine has not been reported in the available literature. The multi-lumped temperature overall energy balance (OEB) is validated with experimental data obtained from a dedicated ORC test stand. A comparison between single-lumped and multi-lumped temperature approaches on the performance predictions is provided along with a discussion about the losses distribution inside the machine.

1. INTRODUCTION

Deterministic models of single-screw compressors (SSC) and expanders (SSE) have been published in literature. One of the first computer models reported in the literature was proposed by Bein and Hamilton (1982) for a low pressure oil-flooded single-screw air compressor. An iterative approach based on a polytropic transformation was used to correlate internal predictions with empirical values. Leakage paths were also considered, neglecting the two-phase flow through the gaps. The heat transfer between the air in the compression chamber and oil was neglected. Successively, Boblitt and Moore (1984) presented a FORTRAN-based computer model of an oil-flooded SSC operating at 100% capacity at matched discharge pressures, meaning the pressure at the end of the compression process corresponded exactly with the discharge pressure. The model is based on two empirical parameters, i.e. polytropic compression efficiency and the discharge flow coefficient. The included leakage model is based on the model proposed by Bein and Hamilton (1982), with the addition of the effect of the oil on the volumetric and isentropic efficiency. However, it was assumed that only oil was leaking from the groove tip sealing lines and the refrigerant leakages were restricted to the the discharge port. The heat transfer between the refrigerant and oil in the closed compression process was neglected. The oil injection process was also included in the model. A total of six control volumes were introduced to analyze the overall compression process. Thermal interactions between each control volumes were modeled by means of a steady-state steady-flow First Law analysis. The closed compression process was divided into a number of steps corresponding to a pressure increment, since the discharge state of a groove had to match the discharge pressure. The main rotor rotation step was a result of the model. Wu and Jin (1988) and Hirai et al. (1986) included additional gas-oil mixture effects into their compressor models as well as the analysis of a slide valve mechanism.

More recently, Wang et al. (2016) presented a detailed thermodynamic model of a SSC with multi-column meshing profile in which continuity and energy conservation equations were applied to the refrigerant gas and lubricant oil. The control volume analysis was applied to a single working chamber by assuming that all the others behaved in a

similar manner. Suction gas heating due to the presence of the motor was also included. A two-phase flow model was employed to calculate the flow rate through the discharge port. A correction coefficient was introduced based upon experimental data. The heat transfer within the working chamber was modeled by including a correction factor to account for the helical shape of the groove. Cooling capacity and shaft power were validated with experimental data. The same authors extended the chamber model to investigate the effect of liquid refrigerant injection to reduce the discharge temperature and to improve the compressor performance (Wang et al. (2018)).

With respect to expanders, Ziviani et al. (2014) and Shen et al. (2018) developed comprehensive models of single-screw expanders for organic Rankine cycle applications by accounting for both leakage and frictional losses. The models have been used to predict the performance of the machines and to determine the effect of leakage gaps and operating conditions on the overall performance.

By analyzing all the models proposed in literature, the overall energy balance of the single-screw machine is not well addressed especially in the case of hermetic or semi-hermetic designs. Ziviani et al. (2014) enforced a single-lumped temperature energy balance to estimate the heat losses through the shell. However, such approach, although effective, is not sufficient to have better understanding of the thermal interactions inside the machine as well as identifying the thermal losses.

In this paper, a detailed overall housing energy balance with a multi-lumped temperature thermal network is proposed and integrated into the detailed expander model. An 11 kWe single-screw expander working with R245fa has been selected as test case to validate the model and perform analyses. The experimental data points of the expander are available from a previous study (Ziviani et al. (2016)).
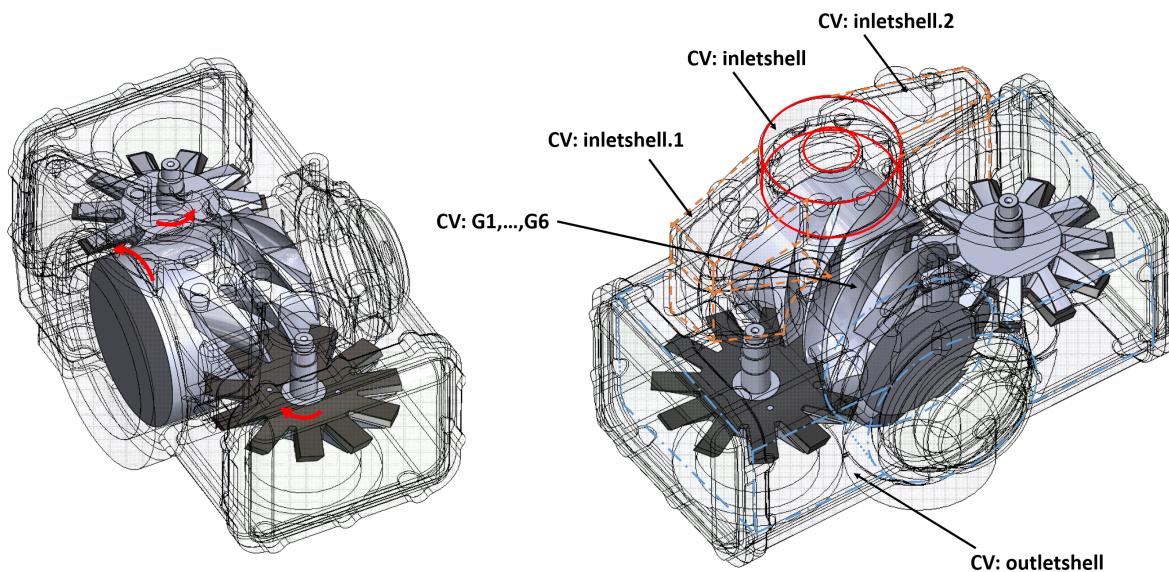

Figure 1: Views of the single-screw expander assembly with the direction of rotation of meshing pair (left) and the control volumes (right).

2. NON-SYMMETRIC MODELING APPROACH

The operating principle of a single-screw expander is based on the simultaneous filling of the grooves on both sides of the main rotor through ports located on the internal cylindrical surface of the housing which hosts the main rotor. As a groove rotates, it is exposed to the suction port until the trailing edge passes over the port. Once the portion of the groove limited by the engaging tooth, by the three sides of the groove and the housing wall is filled with working fluid, the closed expansion occurs until the tooth starts disengaging the groove, when the discharge process begins. Such process occurs on both sides of the main rotor and therefore, when a groove is discharging on one side, it is filling on the other side at the same time. Each groove is employed twice per revolution. By looking at Figure 1, the main rotor

has six grooves, but due to the fact that two starwheels are engaged at the same time, there are six working chambers on each side of the rotor, as mentioned by Wang et al. (Wang et al., 2016). To reduce the complexity of the model, it is common practice to consider only one side of the rotor due to symmetry. A more general approach is adopted in this work. In particular, a non-symmetric description of the machine is considered by computing the expansion process in both sides of the rotor. By referring to Figure 1, the housing has been divided into four static control volumes (CV) which are associated with the common inlet volume, the two internal ducts that connects the inlet to the suction pockets and shell volume connected to the outlet of the expander. On each side of the rotor, six dynamic control volumes which are changing according to the rotation angle are representative of the six working chambers. The rotation of the main rotor is taken as reference. To relax the notation, the rotation angle of the main rotor, θ_{sr}, will be referred to as θ, unless specified. A summary of the control volume definitions is available in Table 1

Table 1: Definition of the different control volumes in the single-screw expander.

Type	Description	Geometry
Static	inletshell	$V = 69$ cm^3, dV $= 0$ cm^3
	inletshell.1	$V = 70$ cm^3, dV $= 0$ cm^3
	inletshell.2	$V = 120$ cm^3, dV $= 0$ cm^3
	outletshell	$V = 569$ cm^3, dV $= 0$ cm^3
Dynamic	G1,...,G6	$V=V(\theta)$, dV=dV(θ) (Ziviani et al. (2018))

The complete evolution of the control volumes over one rotation of one side the main rotor is shown in Figure 2. The control volume G_1 is taken as reference. To be noted is that the remaining control volumes $G_2 \sim G_6$ (solid lines) are phased by $(j\gamma i)_{j=1,2,3,4,5}$ and when each of them complete the revolution, they start wrapping on the opposite of the rotor. At the same time, as new teeth start engaging after G_1, new control volumes form from the groove that ended the expansion process on the other side of the rotor (dashed lines). The present model handles all the CVs on both sides simultaneously with no simplifications due to symmetry.
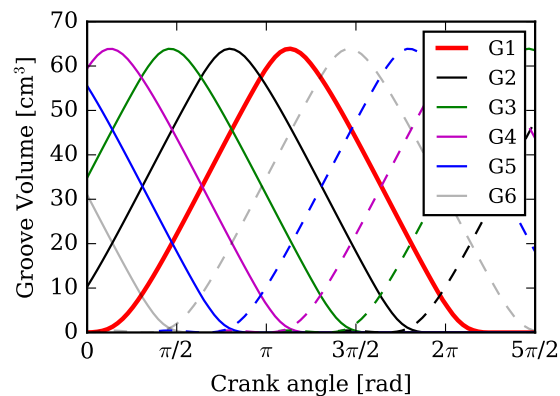

Figure 2: Evolution of the main rotor control volumes over one complete rotation for one side of the main rotor.

The system of governing equations that expresses the conservation of total mass in the control volume, the conservation of the oil mass and the conservation of energy for the general control volume are given as follows: Sub-models for estimating the flow interactions between the working chambers and heat transfer model are necessary in order to carry on the integration.

3. OVERALL ENERGY BALANCE

An overall energy balance of the expander housing is necessary to close the mechanistic model. In particular, thermal interactions occur between the elements of the housing the working fluid during the entire expansion process. Thus, the wall temperatures need to be estimated in order to calculate the associated heat transfer terms. Single-lumped temper-

ature and multi-lumped temperatures are commonly used to enforce the overall energy balance depending on the complexity required. The single-screw expander is an open-drive machine and both approaches are implemented.
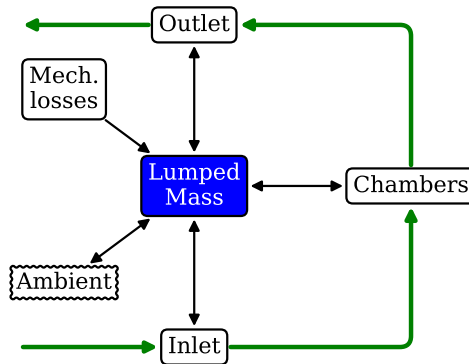

Figure 3: Schematic of the single-lump overall energy balance of the open-drive single-screw expander.

3.1 Single-lumped Temperature

The overall energy balance based on a single-lumped implied that all the expander elements are grouped into one lumped mass having a temperature T_{lump}. Since spatial gradients are neglected, the lumped temperature is uniform. The working fluid exchanges heat with the lumped mass during suction, closed expansion and discharge processes. The heat generated by friction is also assumed to interact with the lumped mass. Last, the lumped mass exchanges heat with the ambient. The overall energy balance for a single lumped element can be written as,

$$\overline{\dot{W}}_{\text{mech,loss}} + \sum_i \dot{Q}_i(T_{\text{lump}}) = 0 \tag{1}$$

where T_{lump} is the mean temperature of the lumped mass of the expander shell and $\dot{Q}_i$ represents all the heat transfer interaction terms between the different parts of the expander and the housing. By referring to Figure 3, the overall energy balance for the single-screw expander is given by:

$$\overline{\dot{W}}_{\text{mech,loss}} + \overline{\dot{Q}}_{\text{cyl,lump}} + \dot{Q}_{\text{inletshell,lump}} + \dot{Q}_{\text{outletshell,lump}} + UA_{\text{amb}}(T_{\text{lump}}) = 0 \tag{2}$$

where the average value of the overall heat transfer coefficient UA_{amb} is obtained from experimental data or assumed accordingly.

3.2 Multi-lumped Temperature

In the multi-lumped temperature approach, the entire expander is divided into different elements, i.e., the lumps. It is assumed that there is no temperature gradient in the individual expander elements, i.e., the lumped temperature analysis method is used. The higher the number of elements identified, the more complex the thermal network model becomes. The overall energy balance model developed for the single-screw expander is based on previous models applied to rolling piston, scroll and reciprocating compressors (Liu, 1994; Chen, 2000; Kim, 2005). The schematic of the overall energy balance of the single-screw expander and the corresponding thermal resistance network are given in Figure 4(a) and Figure 5.

As shown in Figure 5, there are six unknown temperatures: the shell temperature, T_{shell}; temperature of refrigerant gas in the housing, $T_{\text{gas,shell}}$; side plate temperatures, T_{plate}; suction temperatures, $T_{\text{pipe1,suc}}$ and $T_{\text{pipe2,suc}}$; cylinder wall temperature, $T_{\text{cyl,wall}}$. To be noted is that the temperature of the gas within the shell corresponds to the temperature associated with the control volume *outletshell*. The amount of heat lost to the environment due to natural convection is dependent on the temperatures of the housing according to Newton's law of cooling. In order to derive the stedy-state energy balance equations for each lumped-element, the following conventions are imposed (Padhy, 1992):

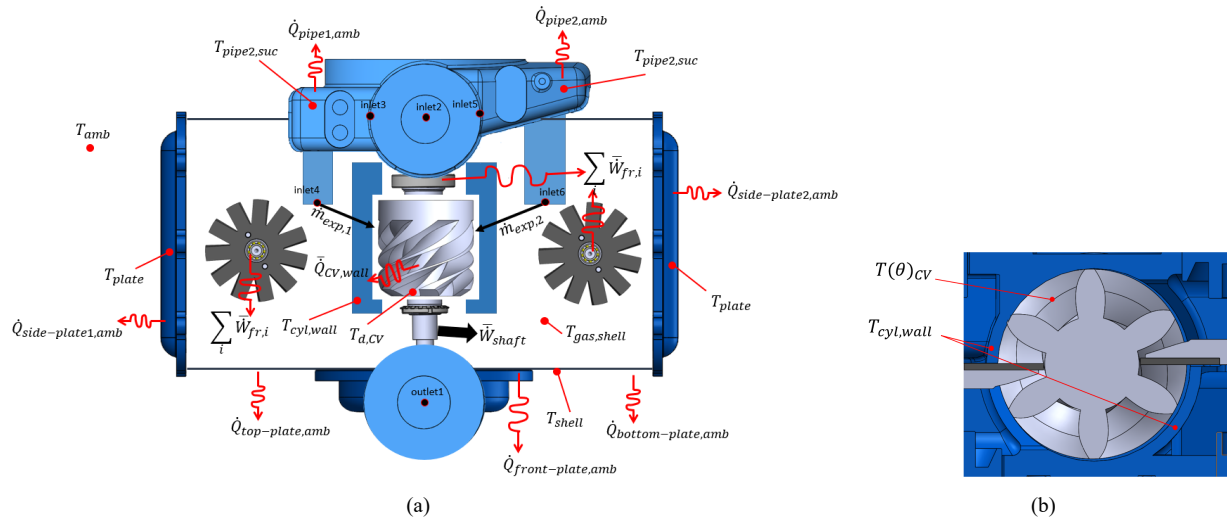- heat addition to an element is considered positive;

Figure 4: (*a*) Schematic of the overall energy balance of the single-screw expander; (*b*) heat transfer between the mixture of refrigerant and oil in the working chambers and the cylinder wall.

- heat transferred from the element is considered negative;
- internal heat generation which includes frictional heat generation is considered positive.
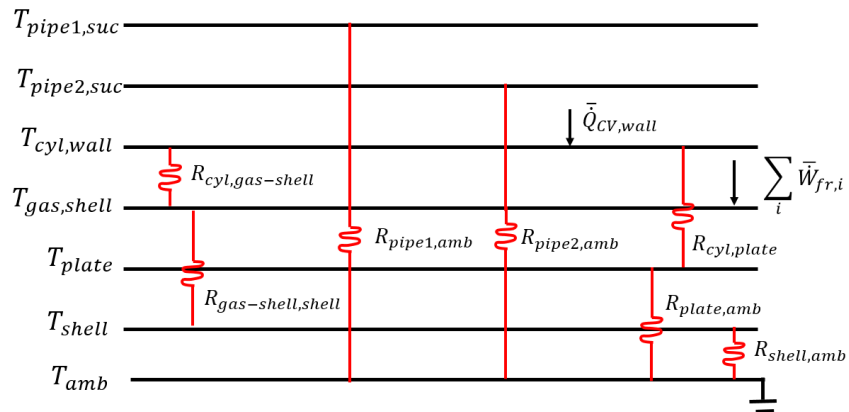

Figure 5: Thermal resistance network of the overall energy balance for single-screw expander.

By applying the energy conservation law to each component, the following equations can be derived:

$$\dot{m}_{\text{exp},1} \left(h_{\text{su},2} - h_{\text{su},4} \right) - \dot{Q}_{\text{pipe1,amb}} = 0 \tag{3}$$

$$\dot{m}_{\text{exp},2} \left(h_{\text{su},2} - h_{\text{su},6} \right) - \dot{Q}_{\text{pipe2,amb}} = 0 \tag{4}$$

$$\dot{m}_{\text{exp},1} \left(h_{\text{su},4} - h_{\text{dis}} \right) + \dot{m}_{\text{exp},2} \left(h_{\text{su},6} - h_{\text{dis}} \right) = \dot{W}_{\text{pV}} + \overline{\dot{Q}}_{\text{cyl,wall}} \tag{5}$$

$$\dot{m}_{\text{exp}} \left(h_{\text{dis}} - h_{\text{out},1} \right) = \dot{W}_{\text{friction}} - \dot{Q}_{\text{gas,shell}} \tag{6}$$

$$\dot{Q}_{\text{cyl,wall}} = \dot{Q}_{\text{top-plate,amb}} + \dot{Q}_{\text{bottom-plate,amb}} \tag{7}$$

$$\dot{Q}_{\text{gas,shell}} = \dot{Q}_{\text{side-plate1,amb}} + \dot{Q}_{\text{side-plate2,amb}} + \dot{Q}_{\text{front-plate,amb}} \tag{8}$$

By referring to Figure 4(b), the groove is approximated as a helical tube with non-circular cross section. The convective heat transfer coefficient is obtained by correcting the Dittus-Boelter correlation to account for the groove geometry.

Similar approach has been adopted for example by Bell (Bell, 2011) in the case of the spiral geometry of the scroll wraps and by Mathison et al. (2008) in the case of curved surfaces in two-stage rotary compressor. The final expression of the heat transfer coefficient is given by:

$$h_{groove} = 0.023 \frac{k_{mix}}{r_{sw} - \frac{d_{sr,sw}}{cos\theta}} Re_{mix}^{0.8} Pr_{mix}^{0.4} \frac{D_h}{d_{eq,groove}} \left\{ 1 + 1.77 \frac{r_{sw} - \frac{d_{sr,sw}}{cos\theta}}{r_{sw} - \frac{1}{2}\left(r_{sw} - \frac{d_{rmsr,sw}}{cos\theta}\right)} \right\} \tag{9}$$

where $d_{eq,groove}$ represents the equivalent diameter of the groove and D_h is the hydraulic diameter of the groove calculated as:

$$D_h = \frac{4V_{groove}(\theta)}{A_{groove}(\theta)} \tag{10}$$

The Reynolds number of the mixture in the screw groove is calculated by considering as mean velocity the peripheral velocity evaluated at the groove center radius between tip and bottom. The instantaneous heat transfer rate between the mixture and the cylinder wall is thus obtained as:

$$\dot{Q}_{cyl,wall}(\theta) = h_{groove} A_{cyl,wall}(\theta) \left[T_{cyl,wall} - T(\theta) \right] \tag{11}$$

Finally, the average heat transfer between the mixture in the working chambers and the cylinder walls over one rotation is obtained from:

$$\overline{\dot{Q}}_{cyl,wall} = \frac{1}{2\pi} \int_0^{2\pi} \left[\sum_{CV} \dot{Q}_{CV} \right] d\theta \tag{12}$$

where the integration is done numerically with a trapezoidal rule.

The heat transfer rate terms $\dot{Q}_{pipe1,amb}$, $\dot{Q}_{pipe2,amb}$, $\dot{Q}_{top-plate,amb}$, $\dot{Q}_{bottom-plate,amb}$, $\dot{Q}_{side-plate1,amb}$, $\dot{Q}_{side-plate2,amb}$, $\dot{Q}_{front-plate,amb}$ and $\dot{Q}_{gas,shell}$ are expressed in the form:

$$\dot{Q} = \frac{T_a - T_b}{R_{ab}} \tag{13}$$

where, $T_a - T_b$ is the temperature difference between two elements and R_{ab} is the heat transfer thermal resistance. In order to find the thermal resistances, empirically correlated averaged Nusselt numbers are calculated.

The cylinder walls exchange heat with the gas within the shell by free convection as well as with the upper and lower surfaces of the housing by conduction. Thus, the thermal conductance of the heat transfer between cylinder wall and housing is given by:

$$UA_{cyl-wall,upper-plate} = \frac{2\pi k_{iron} L_{upper-plate}}{log\frac{r_{upper-plate}}{r_{cyl-wall}}} \tag{14}$$

where k_{iron} is the thermal conductance of the cast iron housing approximated as 70 W/(mK).

There are five types of free convection heat transfer mechanisms that can be identified on the single-screw housing:

- the heat transfer over the upper surface of a plate,
- over the lower surface of a plate
- along a vertical plate,
- along a horizontal pipe
- and that along a vertical pipe.

For each free convection heat transfer type, adequate correlations for the Nusselt number needs to be defined (Incropera & Dewitt, 2002). In particular, for the free convection over the upper surface of a plate:

(a) hot plate, $T_s > T_{inf}$

$$\overline{Nu_L} = 0.54 Ra_L^{1/4} \left(10^4 \leq Ra_L \leq 10^7 \right) \tag{15}$$

(b) cold plate, $T_s < T_{inf}$

$$\overline{Nu_L} = 0.27 Ra_L^{1/4} \left(10^5 \leq Ra_L \leq 10^{10} \right) \tag{16}$$

For the free convection over a lower surface of a plate:

(a) hot plate, $T_s > T_{inf}$

$$\overline{Nu_L} = 0.27Ra_L^{1/4} \left(10^5 \leq RaL \leq 10^{10} \right) \tag{17}$$

(b) cold plate, $T_s < T_{inf}$

$$\overline{Nu_L} = 0.15Ra_L^{1/3} \left(10^7 \leq Ra_L \leq 10^{11} \right) \tag{18}$$

Churchill and Chu (Churchill & Chu, 1975) proposed a correlation to calculate the averaged Nusselt number for the free convective heat transfer along a vertical plate over the entire range of Rayleigh number, Ra_L:

$$\overline{Nu} = \left\{ 0.825 + \frac{0.387Ra_L^{1/6}}{\left[1 + \left(\frac{0.492}{Pr} \right)^{9/16} \right]^{8/27}} \right\}^2 \tag{19}$$

In the case of laminar flow, the following correlation is suggested:

$$\overline{Nu} = 0.680 + \frac{0.670Ra_L^{1/4}}{\left[1 + \left(\frac{0.492}{Pr} \right)^{9/16} \right]^{4/9}} \tag{20}$$

For the case of a horizontal pipe

$$\overline{Nu} = \left\{ 0.600 + \frac{0.387Ra_D^{1/6}}{\left[1 + \left(\frac{0.559}{Pr} \right)^{9/16} \right]^{8/27}} \right\}^2 \quad Nu_D \leq 10^{12} \tag{21}$$

where the subscript D refer to the diameter of the pipe. Sparrow and Gregg (Sparrow & Gregg, 1956) suggested using Equation 19 to calculate the Nusselt number for the free convection along a vertical pipe if the following condition is satisfied:

$$\frac{D}{L} \geq \frac{35}{Gr_L^{1/4}} \tag{22}$$

where D is the pipe diameter, L is the pipe length and Gr_L is the Grashof number. The following modification factor should be used to multiply the averaged Nusselt number if the above condition is not satisfied:

$$F = \frac{1}{3} \left[\frac{L/D}{1/Gr_L} \right]^{1/4} + 1 \tag{23}$$

In all the free convection cases, the so-called film temperature is used to determine the fluid thermal properties which can be defined as:

$$T_f = \frac{T_s + T_{inf}}{2} \tag{24}$$

where T_s is the surface temperature and T_{inf} is the temperature of the ambient or working fluid depending on the case.

Finally, the overall energy balance of the expander that must be satisfied is given by,

$$\overline{W}_{exp,shaft} = \dot{m}_{exp} \left(h_{su,2} - h_{out,1} \right) - \sum_i \dot{Q}_i \left(T_{amb} \right) \tag{25}$$

where $\dot{Q}_{i,amb} \left(T_{amb} \right)$ represents the $i - th$ heat transfer loss through the housing (see Equations 3 to 8).

The system of non-linear equations is solved by employing a modified Broyden's method (Bradie, 2006) to ensure proper bounding of the lumped temperature values.
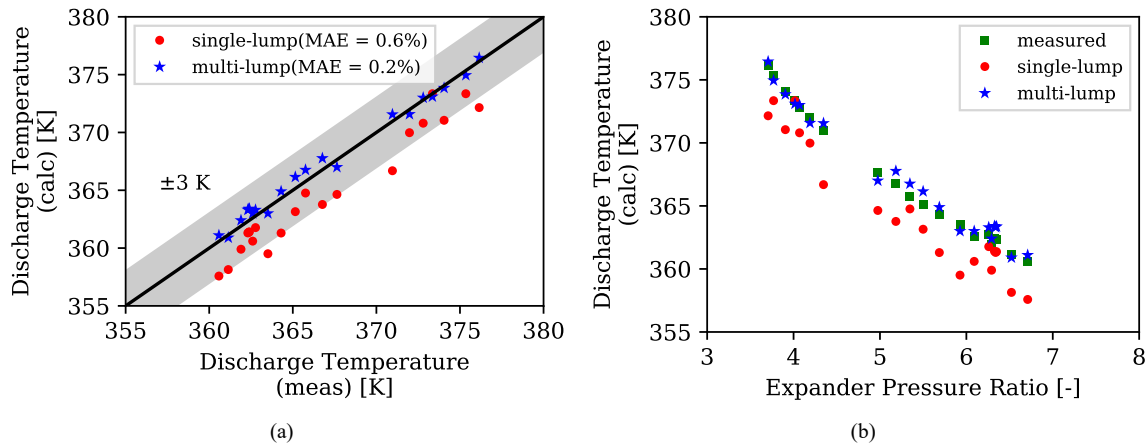
Figure 6: Comparison between measured and calculated discharge temperature by employing single-lump and multi-lump temperature formulations: (*a*) parity plot; (*b*) discharge temperature as a function of the pressure ratio across the expander.
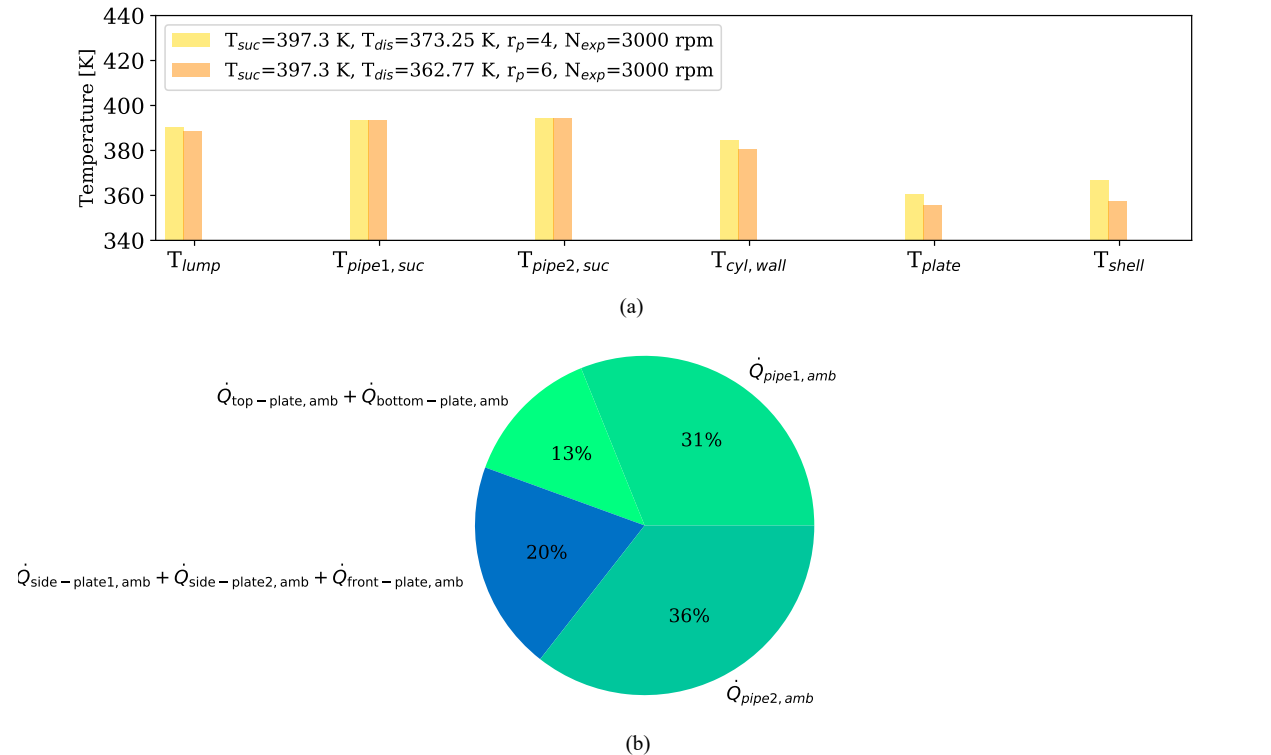

Figure 7: (*a*) Comparison between single-lump temperature (T_{lump}) and multi-lump temperatures models for two operating conditions; (*b*) averaged heat losses distribution.

4. RESULTS AND DISCUSSION

The performance characterization of the single-screw expander installed in an organic Rankine cycle has already been described in Ziviani et al. (2016). The heat source inlet temperature has been kept constant at 125 °C and two working fluids have been tested, i.e. R245fa and SES36, at different pressure ratios and operating conditions. An in-depth validation of the mechanistic model in terms of mass flow rate, discharge temperature, power output, and overall

isentropic efficiency has been proposed in Ziviani et al. (2017). By using the data set of R245fa, the single-lumped temperature formulation and the detailed thermal network model are compared in terms of accuracy in predicting the discharge temperature of the expander. In particular, Figure 6(a) shows the comparison between measured and calculated discharge temperatures with both numerical approaches. Generally, it can be seen that the single-lump model underpredicts the discharge temperature which is related to an overestimation of the heat losses through the housing. The multi-lumped temperature model improved significantly the overall predictions of the mechanistic model. The accuracy of the model can also be appreciated by looking at Figure 6(b), where the discharge temperatures are plotted as a function of the pressure ratios. The detailed thermal-network is able to capture the physical behavior of the expander more consistently.

The two modeling approaches have been further exercised to predict the temperatures of the expander housing. Such analysis has been conducted by considering two operating conditions having the same suction temperature and different pressure ratio. The operating conditions and the results are reported in Figure 7(a). It can be seen that the single-lump temperature model converges to housing temperatures closer to the suction temperature. The UA$_{amb}$ can be tuned to improve the predictions on the discharge temperatures. However, the multi-lump temperature model allows to better understand the temperature distribution of the housing. As expected in the real system, the inlet pipes present a higher surface temperatures than the discharge side. The cylindrical walls surrounding the main rotor have an intermediate temperature level determined by the closed expansion process. The averaged heat losses distribution through the housing of the expander is shown Figure 7(b).

5. CONCLUSIONS

In this paper, a detailed thermal model of an open-drive single-screw expander have been described and integrated into a comprehensive mechanistic model. The following conclusions can be drawn:

- the detailed thermal network model improved the predictions of the expander discharge temperatures;
- the single-lumped temperature approach leads to higher shell temperatures. Whereas, by considering different lumped-temperatures, the model is able to predict higher surface temperatures in the suction side and lower temperatures in the rest of the housing. As part of future work, multiple temperature sensors will be installed to further validated the detailed thermal network;
- the thermal network developed can be easily extended to account for hermetic or semi-hermetic single-screw designs.

NOMENCLATURE

A	area	(m^2)	R	thermal resistance	(K/W)
c	centroid coordinates	(m)	Ra	Rayleigh number	(-)
d	distance	(m)	Re	Reynolds number	(-)
D	diameter	(m)	V	volume	(m^3)
D$_h$	hydraulic diameter	(m)	$\dot{W}$	work rate	(W)
F	force	(N)	θ	crank angle	(rad)
Gr	Grashof number	(-)	ω	angular speed	(rad/s)
h	specific enthalpy	(kJ/kg)	**Subscript**		
	heat transfer coeff.	(kW/(m^{2}K))	amb	ambient	
k	thermal conductivity	(W/(K-m)	CV	control volume	
L	length	(m)	cyl	cylinder	
$\dot{m}$	mass flow rate	(kg/s)	exp	expander	
$\dot{Q}$	heat transfer rate	(kg/s)	dis	discharge	
Nu	Nusselt number	(-)	fr	friction	
Pr	Prandtl number	(-)	out	outlet	
T	temperature	(°C)	s	surface	
r	radius	(m)	su	supply	
			sw	starwheel	

REFERENCES

Bein, T. W., & Hamilton, J. F. (1982). Computer modeling of an oil flooded single screw air compressor. In *International compressor engineering conference.* (Paper 383)

Bell, I. H. (2011). *Theoretical and experimental analysis of liquid flooded compression in scroll compressors* (Unpublished doctoral dissertation). Purdue Univeristy.

Boblitt, W. W., & Moore, J. (1984). Computer modeling of single-screw oil flooded refrigerant compressors. In *International compressor engineering conference.*

Bradie, B. (2006). *A friendly introduction to numerical analysis*. Pearson Prentice Hall, USA.

Chen, Y. (2000). *Mathematical Modeling of Scroll Compressors* (Unpublished doctoral dissertation). Purdue University.

Churchill, S. W., & Chu, H. H. S. (1975). Correlating equations for laminar and turbulent free convection from a horizontal cylinder. *International Journal of Heat and Mass Transfer*, *18*, 1049-1053.

Hirai, T., Noda, S., Sagara, Y., & Tsuzi, K. (1986). Performance analysis of oif single screw compressor. In *International compressor engineering conference.* (Paper 520)

Incropera, F. P., & Dewitt, D. P. (2002). *Fundamentals of heat and mass transfer (5th edition).* Wiley.

Kim, J.-H. (2005). *Analysis of a bowtie compressor with novel capacity modulation* (Unpublished doctoral dissertation). Purdue University.

Liu, Z. (1994). *Simulation of a Variable Speed Compressor with Special Attention to Supercharging Effects* (Unpublished doctoral dissertation). Purdue University.

Mathison, M. M., Braun, J. E., & Groll, E. A. (2008). Modeling of a Two-Stage Rotary Compressor. *HVAC&R Research*, *14*, 719-748.

Padhy, S. K. (1992). Heat transfer model of a rotary compressor. *International Compressor Engineering Conference at Purdue*, Paper 935.

Shen, L., Wang, W., Wu, Y., Lei, B., Zhi, R., Lu, Y., … Ma, C. (2018). A study of clearance height on the performance of single-screw expanders in small-scale organic Rankine cycles. *Energy*, *153*, 45-55.

Sparrow, E. M., & Gregg, J. L. (1956). Laminar free convection heat transfer from the outer surface of a vertical circular cylinder. *Transactions of the ASME*, *78*, 1823-1830.

Wang, Z., Shen, Y., Wang, Z., Wang, J., Jiang, W., & Li, Q. (2018). Theoretical research and optimization analysis for the injection process of the single screw refrigeration compressor. *International Journal of Refrigeration*, *88*, 91-101.

Wang, Z., Wang, Z., Wang, J., Jiang, W., & Feng, Q. (2016). Theoretical and experimental study on thermodynamic performance of single screw refrigeration compressor with Multicolumn Envelope Meshing Pair. *Applied Thermal Engineering*, *103*, 139-149.

Wu, J., & Jin, G. (1988). The computer simulation of oil-flooded single screw compressors. In *International compressor engineering conference.* (Paper 646)

Ziviani, D., Bell, I. H., De Paepe, M., & van den Broek, M. (2014). Comprehensive model of a single screw expander for orc-systems applications. In *22th int.compressor engineering conf. at purdue.*

Ziviani, D., Groll, E. A., Braun, J. E., & De Paepe, M. (2018). Review and Update on the Geometry Modeling of Single-Screw Machines with Emphasis on Expander. *International Journal of Refrigeration*, Accepted.

Ziviani, D., Groll, E. A., Braun, J. E., Horton, W. T., De Paepe, M., & van den Broek, M. (2017). Non-symmetric approach to single-screw expander and compressor modeling. In *Iop conf. ser.: Mater. sci. eng.* (Vol. 232).

Ziviani, D., Sergei, S., Lecompte, S., Groll, E. A., Braun, J. E., Horton, W. T., … De Paepe, M. (2016). Characterizing the performance of a single-screw expander in a small-scale organic Rankine cycle for waste heat recovery. *Applied Energy*, *181*, 155-170.